

PREPARED FOR SUBMISSION TO JHEP

DELPHES 3

A modular framework for fast simulation of a generic collider experiment



DELPHES
fast simulation

J. de Favereau , C. Delaere , P. Demin , A. Giammanco , V. Lemaître , A. Mertens
and M. Selvaggi

*Centre for Cosmology, Particle Physics and Phenomenology (CP3),
Université Catholique de Louvain,*

Chemin du Cyclotron 2, B-1348 Louvain-la-Neuve, Belgium

E-mail: jerome.defavereau@uclouvain.be,

christophe.delaere@uclouvain.be, pavel.demin@uclouvain.be,

andrea.giammanco@uclouvain.be, vincent.lemaitre@uclouvain.be,

alexandre.mertens@uclouvain.be, michele.selvaggi@uclouvain.be

ABSTRACT: The version 3.0 of the DELPHES fast-simulation framework is presented. The tool is written in C++ and is interfaced with the most common Monte-Carlo file formats. Its goal is the simulation of a multipurpose detector that includes a track propagation system embedded in a magnetic field, electromagnetic and hadronic calorimeters, and a muon identification system. The new modular design allows to easily produce the collections that are needed for later analysis, from low level objects such as tracks and calorimeter deposits up to high level collections such as isolated electrons, jets, taus, and missing energy. New features such as pile-up and improved algorithms like the particle-flow reconstruction approach have also been implemented.

Contents

1	Introduction	2
2	Simulation of the detector response	2
2.1	Particle Propagation	2
2.2	Calorimeters	3
2.3	Particle-flow Reconstruction	4
3	Object Reconstruction	5
3.1	Charged leptons and photons	6
3.1.1	Charged leptons	6
3.1.2	Photons	6
3.1.3	Isolation	6
3.2	Jets	7
3.2.1	Jet reconstruction	7
3.2.2	b and τ -jets	7
3.3	Missing transverse energy and scalar transverse energy	8
4	High-level corrections	8
4.1	Jet Energy Scale correction	8
4.2	Pile-up subtraction	9
5	Software implementation	10
5.1	Code structure	10
5.2	Data-Flow	11
5.3	Technical Performance	11
6	Validation	12
6.1	Charged leptons and photons	12
6.2	Jets	14
6.3	Missing Transverse Energy	14
7	Use cases	15
7.1	Top Quark mass	15
7.2	Higgs Production via Vector Boson Fusion with pile-up	17
8	Conclusion	20

1 Introduction

High energy particle collisions can produce a large variety of final states. Highly sophisticated detectors are designed in order to detect and precisely measure particles originating from such collisions. Experimental collaborations often rely on Monte-Carlo event generation for designing and optimizing specific analysis strategies. Whenever such studies require a high level of accuracy, the interactions of long-lived particles with the detector matter content are fully simulated with the GEANT package [1], electronics response is emulated by dedicated routines, and final observables are reconstructed by means of complex algorithms.

This procedure requires expertise and the deployment of large scale computing resources that can be handled only by large collaborations. For most phenomenological studies, such a level of complexity is not needed and a simplified approach based on the parametrisation of the detector response is in general good enough. In 2009, the DELPHES framework was designed to achieve such a goal [2].

DELPHES takes as input the most common event generator output data-formats and performs a fast and realistic simulation of a general purpose collider detector. To do so, long-lived particles emerging from the hard scattering are propagated to the calorimeters within a uniform magnetic field. Photons and charged leptons final observables are computed by smearing the initial momenta according to the resolution of the relevant sub-detectors. High-level reconstructed quantities such as jets and missing energy can be computed either starting from simple calorimeter deposits, or with the so-called particle-flow algorithm.

With respect to its predecessor [2], the present DELPHES version includes a more accurate particle-flow description allowing to combine and optimally use the information of all sub-detectors. This approach is particularly suitable to the treatment of pile-up, which has also been included in DELPHES 3.0. Other features such as b and τ -tagging have been revisited, and it is now possible to apply an energy scale correction on jets. From a technical perspective, the code structure is now fully modular, providing a greater flexibility to the user.

The modeling of the detector, as well as the reconstruction and validation of the physical observables will be described. A general description of the software implementation will be given before discussing a couple of illustrative use cases.

2 Simulation of the detector response

DELPHES simulates the response of a detector composed of an inner tracker, electromagnetic and hadronic calorimeters, and a muon system. All are organized concentrically and symmetric along the beam axis. The user may specify the detector active volume, the calorimeter segmentation and the strength of the uniform magnetic field. Each sub-detector has a specific response, as will be described in the following.

2.1 Particle Propagation

The first step carried by DELPHES is the propagation of long-lived particles within a uniform solenoidal magnetic field. The magnetic field is applied only in the inner tracker volume.

If the particle is neutral, its trajectory will be a straight line from the production point to a calorimeter cell. If it is charged, it will follow an helicoidal trajectory until it reaches the calorimeters. Particles that originate from a point outside the tracker volume are ignored.

Charged particles have a (good) probability to be seen as tracks in the central tracking volume, which provide a direct measurement of their momentum. For simplicity, the angular resolution on tracks is assumed excellent, therefore only a smearing on the norm of the transverse momentum vector is applied at the stage of particle propagation. This hypothesis is valid for most of the past, present and future particle detectors. As for the tracking efficiency, energy and momentum resolutions can be specified by the user and depend on the particle type, transverse momentum and pseudo-rapidity.

2.2 Calorimeters

After propagating in the magnetic field, long-lived particles reach the calorimeters. The electromagnetic calorimeter, ECAL, is responsible for measuring the energy of electrons and photons, while the hadronic calorimeter, HCAL, measures the energy of strongly interacting particles.

In DELPHES, the calorimeters have a finite segmentation in pseudo-rapidity and azimuthal angle (η, ϕ) . The size of the elementary cells can be defined in the configuration file. For simplicity the segmentation is uniform in the transverse direction, and for computational reasons we assume the same granularity for ECAL and HCAL. The coordinate of the resulting calorimeter object, the tower, is computed as the geometrical center of the cell.

Long-lived particles reaching the calorimeters deposit a fixed fraction of their energy in the corresponding ECAL (f_{ECAL}) and HCAL (f_{HCAL}) cells. Electrons, photons and neutral pions leave all their energy in ECAL, while charged pions and other neutral hadrons deposit all their energy in HCAL. Long-lived particle such as kaons, pions and Λ 's are considered stable by most event generators. In DELPHES, such particles are assumed to deposit a fixed fraction of their energy both in ECAL and HCAL. By default, f_{ECAL} is set to 30% and f_{HCAL} to 70% — according to their expected decay products — but this can be tuned by the user. Finally, muons, neutrinos and neutralinos, do not deposit anything in the calorimeters ($f_{ECAL} = f_{HCAL} = 0$).

The resolution of the calorimeters is parametrised as a function of the particle energy and the pseudo-rapidity:

$$\left(\frac{\sigma}{E}\right)^2 = \left(\frac{S(\eta)}{\sqrt{E}}\right)^2 + \left(\frac{N(\eta)}{E}\right)^2 + C(\eta)^2, \quad (2.1)$$

where S , N and C are respectively the *stochastic*, *noise* and *constant* terms. The electromagnetic and hadronic energy deposits are independently smeared by a log-normal distribution with variance σ . The final tower energy is then computed as:

$$E_{Tower} = \sum_{particles} \ln \mathcal{N}(f_{ECAL} \cdot E, \sigma_{ECAL}(E, \eta)) + \ln \mathcal{N}(f_{HCAL} \cdot E, \sigma_{HCAL}(E, \eta)). \quad (2.2)$$

where the sum runs over all particles that reach the given tower, and $\ln \mathcal{N}(m, s)$ is the log-normal distribution with mean m and variance s . A calorimeter tower is also characterized

by its position in the (η, ϕ) plane, given by the geometrical center of the corresponding cell. In order to avoid having to deal with discrete tower positions, an additional uniform smearing of the position over the cell range is performed.

Calorimeter towers are, along with tracks, crucial ingredients for reconstructing isolated electrons and photons, as well as high-level objects such as jets and missing transverse energy.

2.3 Particle-flow Reconstruction

The philosophy of the particle-flow approach is to maximally make use of the information provided by the various sub-detectors for reconstructing the event. This *modus operandi* is adopted by several collaborations (see for example [3]) but intrinsically depends on the specificity of the experimental device. In DELPHES, we opted for a simplified approach based on the tracking system and the calorimeters for implementing the particle-flow event reconstruction.

If the momentum resolution of the tracking system is higher than the energy resolution of calorimeters, it can be convenient to use the tracking information within the tracker acceptance for estimating the charged particles momenta. In real experiments, the tracker resolution will be better than the calorimeter resolution only up to some energy threshold. In DELPHES, if particle-flow reconstruction is switched on, we assume it is always convenient to estimate charged particle momenta via the the tracker.

The particle-flow algorithm produces two collections of 4-vectors — particle-flow tracks and particle-flow towers — that will serve later as input for reconstructing jets and missing transverse energy with a higher resolution. For each calorimeter cell, the algorithm counts:

- N_{calo} , the total number of hits that originate from all long-lived standard model particles propagating within the calorimeter acceptance, provided that at least one among f_{ECAL} and f_{HCAL} is non-zero.¹ Each time the calorimeter cell is reached by such a particle, N_{calo} is incremented by 1. Similarly we define $N_{calo-HCAL}$ ($N_{calo-ECAL}$) which gets incremented if a particle with $f_{HCAL} > 0$ ($f_{ECAL} > 0$) reaches the calorimeter cell.
- N_{trk} , the number of hits that originate from a reconstructed track. Due to tracking inefficiencies, some charged particles will not be reconstructed as tracks, but will produce a hit in a calorimeter cell. By construction $N_{trk} \leq N_{calo}$. We also define $N_{trk-HCAL}$ ($N_{trk-ECAL}$) which is incremented if a charged particle reconstructed as a track with $f_{HCAL} > 0$ ($f_{ECAL} > 0$) reaches the calorimeter cell.

The following two scenarios may occur, $N_{calo} = N_{trk}$ and $N_{calo} > N_{trk}$. The first case is trivial and corresponds to a scenario where the calorimeter cell has been hit only by charged particles that have produced a track. If the particle-flow algorithm is switched on, each track associated to this particular cell will result in a particle-flow track. In this case no particle-flow tower is produced. Here we choose to simply make use of the superior

¹Muons, neutrinos and neutralinos do not deposit any energy in the calorimeters.

energy and momentum resolution of the tracking system for estimating the charged particles 4-momenta.

The second case occurs when either one or more neutral particles did produce a hit in the calorimeter cell, or when at least one charged particle did not result in a reconstructed track. The most trivial occurrence is when $N_{trk} = 0$, which means that only neutrals and mis-reconstructed charged particles have produced a hit. In this case the particle-flow algorithm will trivially produce a single particle-flow tower. If $N_{trk} > 0$ there are two possibilities that need to be treated separately:

- if the calorimeter cell is hit only by particles that deposit their total energy either in ECAL or in HCAL it is convenient to consider the two calorimeter sub-components independently. This translates into the condition $N_{calo-ECAL} + N_{calo-HCAL} = N_{calo}$. Moreover, if at least one of the calorimeter sub-components is hit exclusively by particles associated with a reconstructed track, that is, $N_{calo-ECAL} = N_{trk-ECAL}$ (or $N_{calo-HCAL} = N_{trk-HCAL}$), then such tracks get stored as particle-flow tracks. All remaining HCAL (or ECAL) hits will result in a single particle-flow tower. The energy of the particle-flow tower is obtained by smearing according to the HCAL (ECAL) resolution alone. These cases correspond for instance to a calorimeter cell being hit by an electron and a neutron (or by a charged pion and a photon).
- if the previous conditions are not satisfied, only one particle-flow tower (and no particle flow-tracks) is produced. This 4-vector has the energy of the full tower, obtained by applying the procedure explained in equation (2.2). This case occurs frequently when one sub-detector (HCAL or ECAL) is hit both by a neutral and a charged particle. In this case, the neutral energy would have to be indirectly calculated by subtracting the charged energy from the total calorimeter energy. The resolution on the total energy taken directly from the calorimeter, or calculated by adding the charged and neutral component, will be exactly the same. It is therefore useless to consider separately these two components in this case. Therefore we simply take as final particle-flow object the full calorimeter tower.

The output of the particle-flow algorithm consists in two collections of objects. The particle-flow tracks contain charged particles estimated with a good resolution. The particle-flow towers contain in general a combination of charged and neutral particles, and are characterized by a lower resolution. As will be shown in sections 3.2 and 4.2, besides producing high-resolution inputs for jets and missing transverse energy, the particle-flow approach can be pretty useful for addressing pile-up subtraction. While very simple when compared to what is actually required in real experiments, the algorithm described above is shown to reproduce well the performance achieved at LHC later in section 6.

3 Object Reconstruction

In DELPHES, the object reconstruction and identification is based on a series of approximations to sensibly speed up the procedure while keeping a good accuracy.

3.1 Charged leptons and photons

3.1.1 Charged leptons

Taus Hereafter, since τ leptons decay before being detected, we refer by charged leptons solely to electrons (e^\pm) and muons (μ^\pm). The reconstruction of hadronically decaying τ 's will be addressed in section 3.2.2, while leptonic τ decays can be indirectly studied from the decay products when processing the DELPHES output.

Muons In a generic collider detector, muons are usually reconstructed by combining the inner tracking system and muon chambers information. Due to their minimally ionizing nature, muons are often considered as the cleanest objects to reconstruct.

In DELPHES, a muon originating from the interaction, has some probability of being reconstructed, according to the user defined efficiency parametrisation. This probability vanishes outside the tracker acceptance, and for muon momenta below some threshold. The latter requirement enforces that looping particles are not stored in the output collection. The final muon momentum is obtained by a Gaussian smearing of the initial 4-momentum vector. The resolution is parametrised as a function of p_T and η by the user.

Electrons The reconstruction of electrons is non-trivial in a typical collider experiment. By interacting with the detector material and the magnetic field, electrons originating from the hard scattering may lose a significant fraction of their energy by *brehmsstrahlung* radiation. The full electron reconstruction usually involves combining information from the tracking system together with the electromagnetic calorimeter. In DELPHES, we circumvent these reconstruction complexities by parametrising the combined reconstruction efficiency as function of the energy and pseudorapidity. For the electron energy resolution, we use a combination of the ECAL and tracker resolution. At low energy, the tracker resolution dominates, while at high energy, the ECAL energy resolution dominates.

3.1.2 Photons

The reconstruction of photons relies solely on the ECAL. Photon conversions into electron-positron pairs are neglected. The final photon energy is obtained applying the ECAL resolution function presented in section 2.2. All photons that reach the ECAL are reconstructed in DELPHES. In addition, electrons that fail to be reconstructed as tracks and neutral pions (π^0) are automatically classified as photons.

3.1.3 Isolation

An electron, muon or photon is *isolated* if the activity in its surrounding is small enough. Requiring an object to be isolated reduces the probability that it originates from a jet. Several possible definitions exist for an isolation variable, depending on the particular level of signal-to-background rejection that the analyzer desires to achieve. In DELPHES, we have opted for a simple one. Nevertheless, the modularity of the framework allows the user to adopt alternative definitions that are more suitable to the analysis requirements. For each

reconstructed electron, muon, or photon ($P = e, \mu, \gamma$), we define the isolation variable I as:

$$I(P) = \frac{\sum_{\substack{\Delta R < R, p_T(i) > p_T^{min} \\ i \neq P}} p_T(i)}{p_T(P)}, \quad (3.1)$$

where the denominator is the transverse momentum of the particle of interest P . The numerator is the sum of transverse momenta above p_T^{min} of all particles that lie within a cone R around the particle P , except P . The input particle collection entering the sum can be freely specified by the user. Particle-flow objects, or simply tracks and calorimeter towers are common choices for the input collection entering the isolation variable $I(P)$ calculation. Typically values of $I \approx 0$ indicate that the particle is *isolated*. In DELPHES, P is said to be *isolated* if $I(P) < I_{min}$. The user can specify via the configuration file the three isolation parameters p_T^{min} , R and I_{min} .

3.2 Jets

3.2.1 Jet reconstruction

In a hadron collider experiment, final states are often dominated by jets. An accurate jet reconstruction is therefore crucial. A naive approach would consist in parametrising the jet response from the generated parton to the reconstructed jet. Although very fast, this approach would require constant input for tuning from real experiments and would have to be repeated for each variation of the jet reconstruction algorithms. Moreover, such a parametrisation would suffer from being process dependent and would not easily cope with extra radiation and hadronization effects.

Thanks to the modularity of the version 3 of DELPHES, it is possible to produce jets starting from different input collections:

- *Generated Jets* are clustered from generator level long-lived particles obtained after parton-shower and hadronization. No detector simulation nor reconstruction is taken into account.
- *Calorimeter Jets* use calorimeter towers defined in section 2.2 as input.
- *Particle-Flow Jets* are the result of clustering the particle-flow tracks and particle-flow towers defined in section 2.3.

In addition, the user has the freedom to choose the jet clustering algorithm along with its characterizing parameters, as well as minimum threshold for the jet transverse momentum to be stored in the final collection. The DELPHES framework integrates the FASTJET package [4, 5] and therefore allows jet reconstruction with the most popular jet clustering algorithms developed so far while keeping track of the constituents.

3.2.2 b and τ -jets

Identifying jets that result from τ -lepton decays or the hadronization of heavy flavor quarks — typically b or c -quarks — is crucial in high energy collider experiment as these might

indicate the production of heavy unstable particles. In real experiments, such identification often relies on the combined use of advanced tracking and vertexing techniques, and jet shape and composition information. In DELPHES a purely parametric approach based on Monte-Carlo generator information has been adopted.

The algorithm for b and τ -jet identification proceeds as follows: the jet becomes a potential b -jet or a τ -jet candidate if, respectively, a generated b or τ is found within some distance $\Delta R = \sqrt{(\eta^{jet} - \eta^{parton})^2 + (\phi^{jet} - \phi^{parton})^2}$ of the jet axis. The probability to be identified as b or τ depends on user-defined parametrisations of the b and τ -tagging efficiency. The user can also specify a mis-tagging efficiency parametrisation, that is, the probability that a particle other than b or τ is wrongly identified as a b or a τ . The modularity of the DELPHES framework allows the user to use several b and τ -tagging algorithms for the same jet collection and to easily implement other tagging algorithms, eventually involving an analysis of the jet constituents.

3.3 Missing transverse energy and scalar transverse energy

Partons in the initial state having a negligible transverse momentum, the total transverse energy of undetected particles — the *missing transverse energy* (E_T^{miss}) — can be assessed from the transverse component of the total energy deposited in the detector. This will for example account for neutrinos in the standard model but will be degraded by the detector resolution and limited acceptance in the forward region. Another useful quantity is the so-called *scalar transverse energy sum* (H_T). The definition of these two quantities is as follows:

$$\vec{E}_T^{miss} = - \sum_i \vec{p}_T(i), \quad H_T = \sum_i |\vec{p}_T(i)|, \quad (3.2)$$

where the index i runs over the selected input collection. As for the jets, the E_T^{miss} and H_T variables can be computed starting from different input collections. The *Calorimeter* E_T^{miss} and *Calorimeter* H_T variables are estimated by considering only calorimeter towers, while the *Particle-Flow* E_T^{miss} and *Particle-Flow* H_T use particle-flow candidates as input. These quantities can also be calculated using only generator level information.

4 High-level corrections

So far, we have discussed the procedure in DELPHES for reconstructing and identifying the most common objects in collider experiments. At this stage, the resulting collections are not yet ready for final analysis. Residual effects such as pile-up contamination and non-uniformity in the energy response need to be corrected for. In the following we will show how such effects are dealt within DELPHES.

4.1 Jet Energy Scale correction

The average momenta of reconstructed objects do not always match that of their generator-level counterpart. This effect, observed also in real experiments, is particularly explicit in complex objects such as jets where the total smearing is non-trivial due to the clustering

procedure, and where parts of the generator-levels components, such as neutrinos, muons and looping particles are lost.

In DELPHES non-composite objects display by construction an average response close to unity. The energy scale correction is therefore applied only on jets. The user can apply a jet energy scale correction as a function of the reconstructed jet pseudo-rapidity and transverse momentum.

4.2 Pile-up subtraction

At the LHC, several collisions per bunch-crossing will occur in high luminosity conditions, most of them resulting in a small amount of activity in the detector. Due to the elongated shape of the proton bunches constituting the beams, such additional *pile-up events*, take place in a similarly elongated region (called beam spot) around the nominal interaction point. In DELPHES, pile-up interactions are extracted from a pre-generated low- Q^2 QCD sample. These minimum-bias interactions are randomly placed along the beam axis according to some longitudinal spread that can be set by the user. The actual number of pile-up interactions per bunch-crossing is randomly extracted from a Poisson distribution.

Pile-up directly affects the performance of jets, E_T^{miss} and isolation. In real experiments, pile-up interactions are identified by means of vertex reconstruction. If such interactions occur far enough from the hard interaction, a precise vertexing algorithm is able to detect them. Combining vertexing and tracking information allows to identify contaminating charged particles from pile-up. On the other hand, since neutral particles do not produce tracks, neutral pile-up contamination can only be estimated *on average*. In DELPHES, pile-up subtraction can be done in two steps:

Charged pile-up subtraction We assume that vertices corresponding to pile-up interactions occurring at a distance $|z| > Z_{vtx}$ can be reconstructed. The parameter Z_{vtx} is obviously related to the spatial vertex resolution of the detector. We assume that pile-up interactions occurring at $|z| < Z_{vtx}$ cannot be disentangled from those originating from the high- Q^2 process. Therefore every charged particle originating from such vertices cannot be subtracted from the event, while every charged particle originating from a vertex positioned at $|z| > Z_{vtx}$ can be removed from the event, provided that the corresponding track has been reconstructed. For simplicity, in DELPHES we assume that the track reconstruction efficiency does not vary with the vertex position.

Residual pile-up subtraction Other techniques are needed in order to extract and remove residual contributions: these include particles that are too close to the hard interaction vertex to be identified as pile-up products with tracking information, charged particles that failed track reconstruction and neutral particles. In DELPHES we have opted for the Jet Area method [6, 7]. This approach, widely used in present collider experiments, allows to extract an average contamination density ρ on an event-by-event basis.

The pile-up density ρ , can then be used to correct observables that are sensitive to the residual contamination, mainly the jet energies and the isolation variable (defined in equation (3.1)). In the presence of residual pile-up contamination, these two quantities are

corrected in the following way:

$$p_{jet} \rightarrow p_{jet} - \rho \cdot A_{jet}, \quad (4.1)$$

$$I(P) \rightarrow I(P) - \frac{\rho \cdot \pi R^2}{p_T(P)}, \quad (4.2)$$

where A_{jet} is the jet area estimated via the FASTJET package, and R is the diameter of the isolation cone.

Treating separately the charged and the residual pile-up components is particularly effective if combined with the particle-flow reconstruction approach. For instance particle-flow tracks that are not associated with the hard interaction can be automatically removed from a jet reconstructed with the particle-flow algorithm. The neutral energy offset can then be estimated with the Jet Area method. If no tracking information is available (for *Calorimeter Jets* for instance), one can simply estimate the global event pile-up contribution with the Jet Area Method.

5 Software implementation

DELPHES is a modular framework written in C++ and is based on the ROOT analysis framework [8]. It is fully integrated within the MADGRAPH [9] suite. It makes use of other external libraries such as FASTJET [4], ExRootAnalysis [10] and ProMC [11]. In the following the code structure and technical performance will be discussed.

5.1 Code structure

DELPHES can be subdivided in the following subsystems:

- *Memory manager* minimizes the amount of memory allocations. It allows to create, destroy and clear all data collections used by other services and modules. It also clears all data collections produced by other services and modules between events in the event loop.
- *Configuration manager* stores the parameters for all modules and provides access by name to these parameters.
- *Data manager* provides access by name to all data collections created by other services and modules.
- *Universal object* represents all physics objects (particles, tracks, calorimeter towers, jets) with possibility to add user defined information.
- *Modules* consume and produce collections of universal objects.
- *Readers* read data from different file formats.

The modular system allows to configure and schedule modules via a configuration file, add modules, change data-flow, alter output information. Modules communicate entirely via collections of universal objects. (TObjArray of Candidate four-vector like objects).

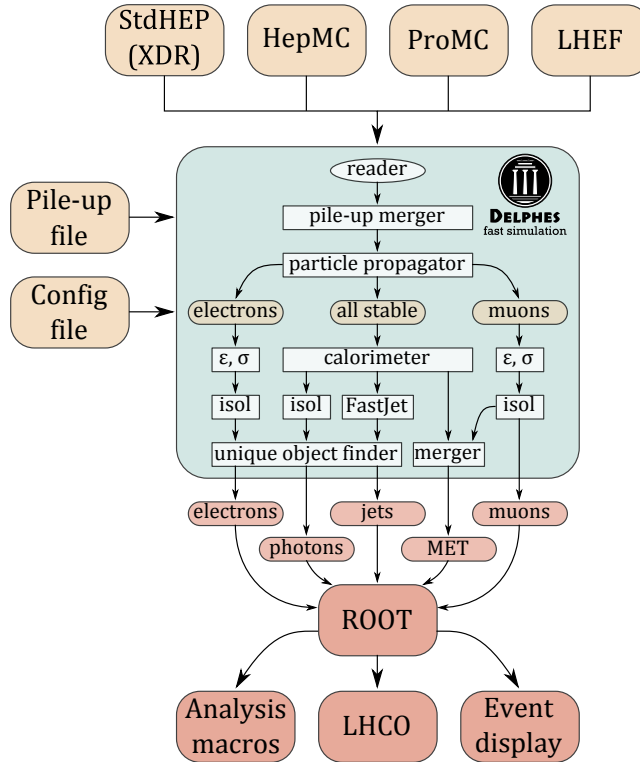


Figure 1. Flow chart describing the DELPHES workflow.

5.2 Data-Flow

A simplified data-flow diagram is shown in figure 1. DELPHES allows to access data from different file formats (ProMC [11], HEPMC [12], STDHEP [13] and the LesHouches event format (LHEF) [14]). Event files coming from external Monte-Carlo generators are first processed by a reader. The Reader converts stable particles into a collection of universal objects. This collection is then processed by a series of modules. Finally, DELPHES allows to store and analyze events in a ROOT tree format [8].

ROOT tree objects are created from particles generated by a Monte-Carlo generator and from objects produced by DELPHES (physics objects like jets, electrons, muons, etc.). For uniformity, each branch is represented by a `TClonesArray`. If a branch contains a single entry per event (for example the E_T^{miss}), the branch is then represented by a `TClonesArray` with only one entry. Objects stored in the tree are linked by means of `TRef` pointers or `TRefArray` (array of pointers). More documentation on the content of the DELPHES output ROOT tree is available on the DELPHES website [15].

5.3 Technical Performance

The main motivation for a tool like DELPHES is to minimize the resources needed on top of those used for event generation: small memory footprint, efficient usage of CPU and small

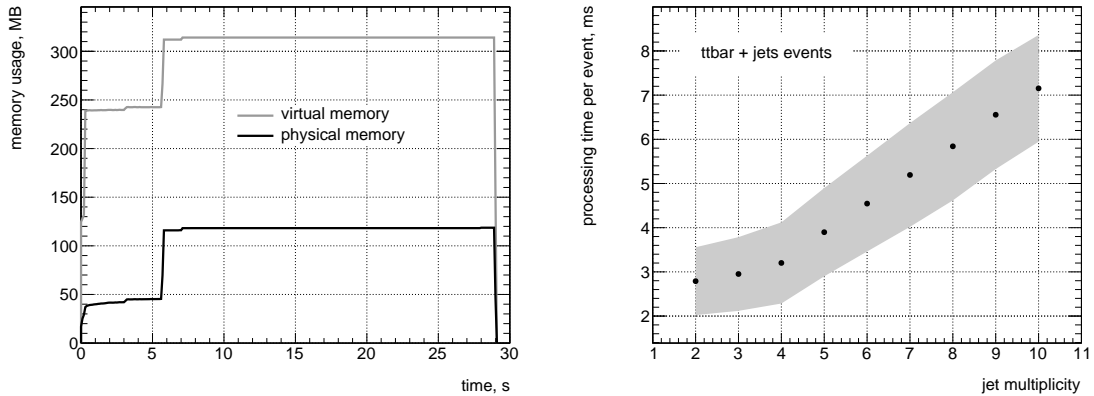


Figure 2. Left: memory usage as function of time after the program start. Right: processing time per event as function of jet multiplicity on inclusive $t\bar{t}$ events.

file size.

Figure 2 illustrates how well DELPHES achieves these goals. Memory usage does not exceed a few hundreds of megabytes and remains constant after the initial memory allocation. Processing time can be as low as a few milliseconds and is expected to follow the scaling law of the underlying jet reconstruction algorithm.

6 Validation

The simulation and reconstruction in DELPHES has to be validated by comparing the resolution of the output objects to the resolutions of real experiments. We chose to validate DELPHES against the two major multipurpose collider experiments, CMS and ATLAS. Only the performance of high-level objects such as electrons, muons, photons, jets and E_T^{miss} , is discussed here. All the Monte-Carlo samples used for the validation are produced with the MADGRAPH5 event generator [9] and hadronized with PYTHIA6 [16]. In order to properly account for tree-level higher order QCD contributions, the k_T -MLM matching procedure was applied [17]. Events are then processed by DELPHES with specific CMS and ATLAS configurations.²

6.1 Charged leptons and photons

Electrons and muons are generated from two independent $p p \rightarrow Z/\gamma^* \rightarrow e^+ e^-$ and $p p \rightarrow Z/\gamma^* \rightarrow \mu^+ \mu^-$ samples, while photons are obtained from a $p p \rightarrow \gamma \gamma$ sample. The resolution is computed as follows. For each generated e^\pm (μ^\pm , γ), we look for the reconstructed e^\pm (μ^\pm , γ) candidate with the smallest $\Delta R = \sqrt{(\eta^{rec} - \eta^{gen})^2 + (\phi^{rec} - \phi^{gen})^2}$. If $\Delta R < 0.2$, the generated particle is paired with a reconstructed isolated particle. The resolution is computed, for each bin, as the Gaussian variance of the distribution of the ratio $(E^{gen} - E^{rec})/E^{gen}$ (or alternatively $(p_T^{gen} - p_T^{rec})/p_T^{gen}$).

²A default CMS and ATLAS configuration card is included within each DELPHES release.

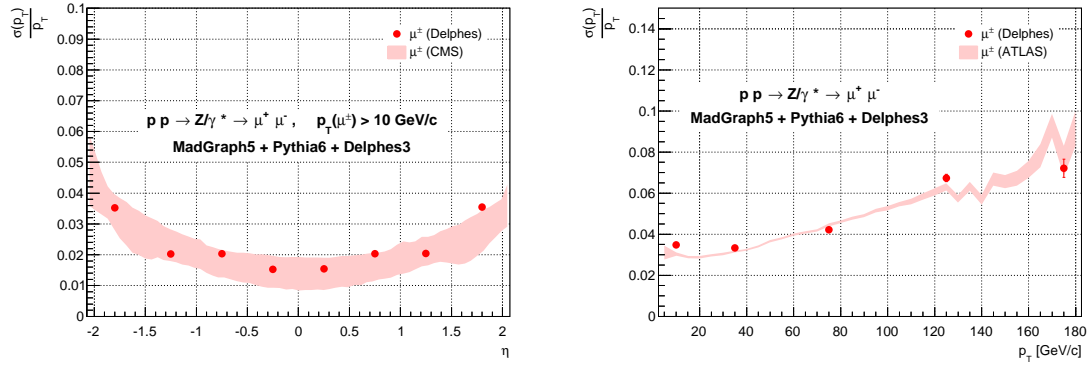


Figure 3. Left: muon p_T resolution as function of η for DELPHES and CMS [18]. Right: muon p_T resolution as function of p_T for DELPHES and ATLAS [19]

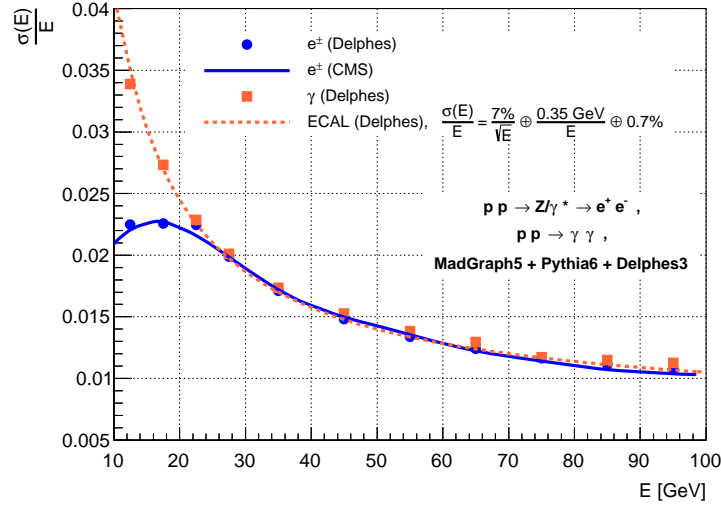


Figure 4. Electron and photon energy resolution as a function of the energy for a CMS-like detector. The CMS electron resolution is from [20].

A comparison of the muon p_T resolution obtained with DELPHES and the CMS [18] and ATLAS [19] detectors is shown in figure 3. The agreement is good for both.

In figure 4 the electron and photon energy resolution are shown. For comparison the electron energy resolution from CMS [20] is also shown. The electron resolution agrees well between CMS and DELPHES. As an illustration, we show also the nominal ECAL resolution in DELPHES. At high energies the electron and photon resolutions match perfectly the ECAL resolution. At low energies, the electron resolution is driven by the tracking resolution.

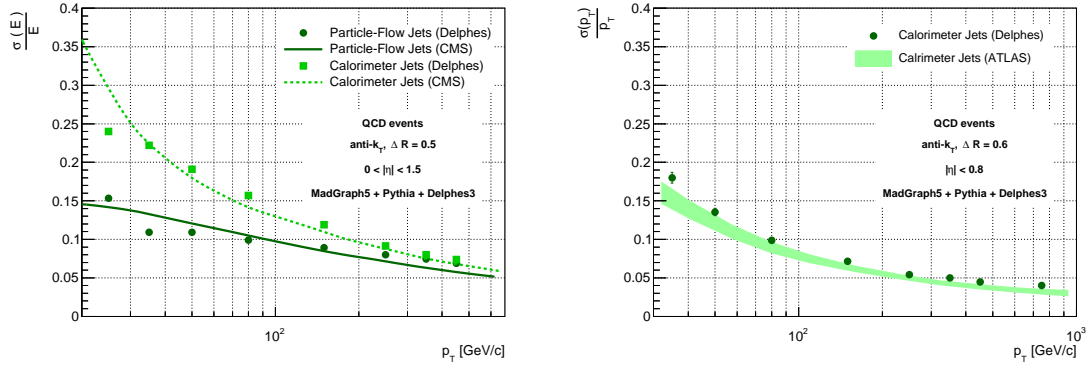


Figure 5. Left: Jet energy resolution of Particle-Flow and Calorimeter jets in CMS [3]. Right: Jet energy resolution of Calorimeter jets in ATLAS [21]

6.2 Jets

The validation of jets is performed on QCD events. The jet energy resolution is obtained in a similar way as explained in section 6.1 by matching reconstructed and generated jets. For both CMS and ATLAS jets are clustered with the anti- k_T algorithm with a cone parameter $\Delta R = 0.5$ and $\Delta R = 0.6$ respectively.

In figure 5 (left) a comparison between CMS and DELPHES resolutions is shown for Calorimeter Jets and Particle-Flow Jets. Both approaches show a good agreement with CMS results [3]. For the ATLAS comparison only Calorimeter Jets resolutions are shown (figure 5 (right)). Also in this case, DELPHES reproduces with good accuracy the ATLAS results [21].

6.3 Missing Transverse Energy

The E_T^{miss} performance is validated both on events with neutrinos (real E_T^{miss}) and without neutrinos (fake E_T^{miss}) in the final state.

Inclusive top pair events are used for testing the real E_T^{miss} performance. The resolution is computed as usual by comparing the E_T^{miss} obtained with calorimeter towers, or particle-flow candidates with the sum of neutrino transverse momenta at parton level. The resolution, as a function of the true E_T^{miss} in the event, is shown in figure 6 (left). Both for the Calorimeter and Particle-Flow E_T^{miss} the agreement between DELPHES and CMS [3] is good.

The fake E_T^{miss} performance is asserted by means of a $Z/\gamma^* \rightarrow \mu^+ \mu^-$ sample. Following the approach of the ATLAS collaboration [22], we select events by requiring the di-muon invariant mass to be compatible with the Z boson mass and we reject events where at least one jet with $p_T > 20$ GeV has been reconstructed. The resolution of the x and y components of the E_T^{miss} as a function of the number of reconstructed primary vertices is shown in figure 6 (right).

Since no vertex reconstruction is performed in DELPHES, the number of reconstructed vertices is simply obtained by rescaling the number of generated pile-up interactions by a

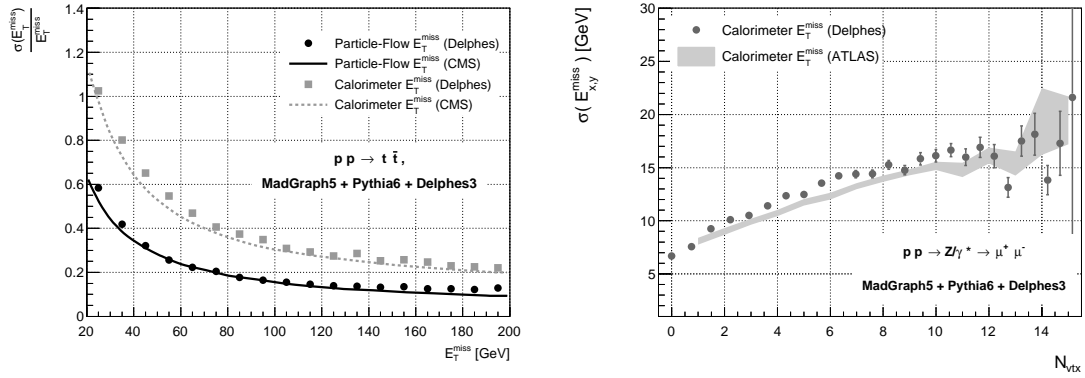


Figure 6. Left: Particle-Flow E_T^{miss} and Calorimeter E_T^{miss} resolution in DELPHES and CMS [3]. Right: $E_{x,y}^{miss}$ resolution in DELPHES and ATLAS as a function of the number of reconstructed primary vertices.

pile-up dependent factor. This factor accounts for the vertex reconstruction efficiency in the presence of pile-up. The vertex efficiency is assumed to decrease linearly as a function of the number of true pile-up interactions. The efficiency varies from 75% at low pile-up (≈ 0) to 50% at high pile-up (≈ 40). These numbers have been extracted from [23].

7 Use cases

In order to illustrate the DELPHES fast-simulation with concrete examples, two use cases will be developed in the following. In the first example, the mass of the top quark will be reconstructed in semi-leptonic $t\bar{t}$ events. The performance of the reconstruction and selection will be compared with the literature. In the second example, the impact of the presence of pile-up on a typical vector boson fusion Higgs analysis workflow will be demonstrated. Both examples are distributed as part of the DELPHES releases and are meant to be easy to understand.

7.1 Top Quark mass

In modern collider experiments at High Energy, $t\bar{t}$ events are among the most common signatures observed in the detectors. When one top quark decays leptonically and the other hadronically, the signature is characterized by one lepton, missing transverse energy and four jets, two of them originating from one b quark. Moreover, at the LHC, about 50% of events have extra hard jets coming from initial or final state radiation. Following the semi-leptonic $t\bar{t}$ analysis described in ref. [24], we will reconstruct the hadronic top-mass.

The $t\bar{t}$ +jets sample has been generated with MADGRAPH5 at a center of mass energy $\sqrt{s} = 7$ TeV and PYTHIA6 was used for parton shower and hadronization. Backgrounds are not considered here. The reconstruction has been performed via DELPHES using the detector configuration designed to mimic the performance of the CMS detector. The analysis has been performed with the help of the DELPHESANALYSIS package [25].

	CMS	DELPHES
correct	15.5 %	15.8 %
wrong	17.4 %	16.7 %
unmatched	67.1 %	67.4 %

Table 1. Fractions of permutations for each type of assignment in the top-mass range 100 to 400 GeV for CMS and DELPHES.

Following the CMS approach, we select events with exactly one isolated lepton (electron or muon) with $p_T > 30$ GeV/c and $|\eta| < 2.1$. In addition, we require at least four jets with $p_T > 30$ GeV/c and $|\eta| < 2.4$. The anti- k_T algorithm with a cone $R = 0.5$ was used for jet clustering. Among the selected jets, at least two must be b-tagged and at least two must be identified as *light jets* (i.e. fail the b-tagging criteria). The b-tagging efficiency parametrisation has been extracted from [26]. The signal efficiency for this selection is 2.8%, compared to 2.3% in the CMS analysis, showing a reasonable agreement between DELPHES and CMS. Given the high jet multiplicity, the signal selection is extremely sensible to changes in requirements that can affect the jet selection. The slight difference in the efficiencies value could be explained by a slight overestimate of the jet energy scale or the b-tagging efficiency.

Since selected events contain two b-jets (b_1 and b_2) and two light jets (j_1 and j_2), among the four leading jets two choices are possible for reconstructing the hadronic top mass: (b_1, j_1, j_2) and (b_2, j_1, j_2) . Each of the two possible assignments can be classified as:

- *unmatched*, if there is at least one of the four observed leading jets that does not match any parton from the top quark decay.
- *wrong permutation*, if the four leading jets match with the four partons but the assignment of the reconstructed b-jet with the b parton originating from the hadronically decayed top leg is wrong,
- *correct permutation* if all the jet-parton assignments are correct.

The relative fraction of each permutation category has been compared with the fractions obtained by the CMS collaboration, showing a good agreement (see table 1). The top quark mass distributions obtained with DELPHES and CMS for the three permutation categories are shown in figure 7 and 8, left. The DELPHES distributions are normalized to the CMS total number of permutations. Overall the shapes corresponding to the three categories are correctly reproduced by DELPHES. However, a slight difference in the mass resolution is observed (see figure 7, left). The worse resolution observed for CMS can be confidently attributed to the fact that CMS data contains a certain amount of pile-up interactions (≈ 9). Pile-up, not considered in the present study, can degrade the jet energy resolution, and in turn the mass resolution.

For the sake of illustration, the reconstructed hadronic top mass using correct permutations only is shown in figure 8 (right) using three different jet collections: *Generated Jets*,

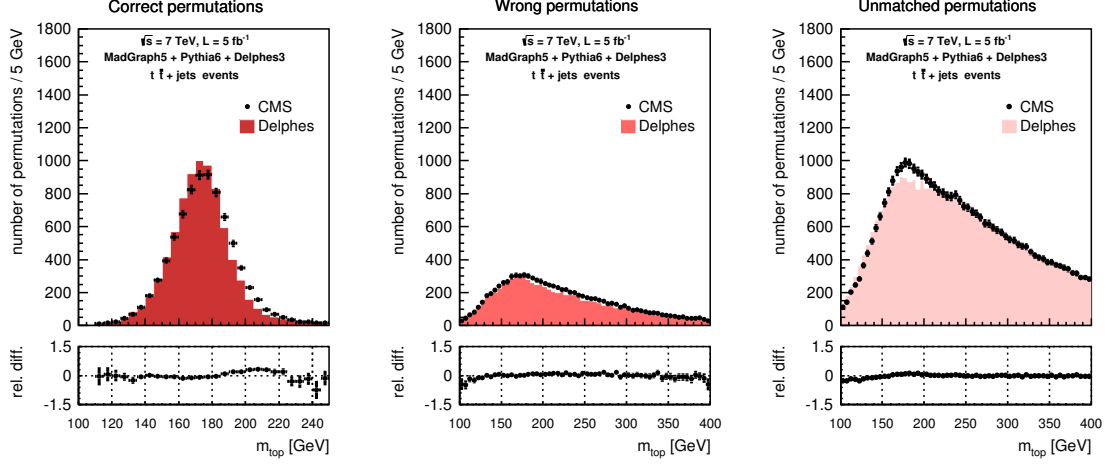


Figure 7. Reconstructed hadronic top mass distributions for the *correct assignments* (left), *wrong assignments* (center) and *unmatched permutations* (right). The DELPHES distributions are normalized to the CMS yield. The CMS contributions are taken from ref. [24].

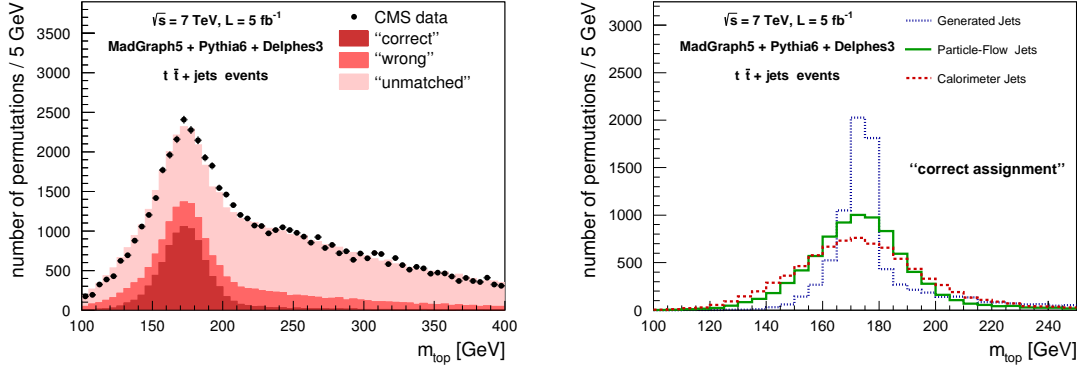


Figure 8. Left: Reconstructed hadronic top mass for all possible assignment categories. The DELPHES distribution is normalized to the CMS yield. The CMS contributions are taken from ref. [24]. Right: Reconstructed hadronic top mass distribution for the *correct assignments* only. The distribution is shown for *Generated Jets*, *Particle-Flow Jets* and *Calorimeter Jets*.

Calorimeter Jets and *Particle-Flow Jets*, defined in section 6.2. We observe, as expected, a narrow peak when using *Generated Jets* and wider peaks when using *Particle-Flow Jets* or *Calorimeter Jets*. This demonstrates the need for using realistically reconstructed objects rather than hadron-level quantities in prospective phenomenological studies.

7.2 Higgs Production via Vector Boson Fusion with pile-up

Searching the Higgs particle produced via Vector Boson Fusion, and decaying to a $b\bar{b}$ pair, can be useful in order to further constrain the VVH and bbH couplings in the standard model. The signal being characterized by a fully hadronic final state, the favorable branching ratio of the $H \rightarrow b\bar{b}$ decay is heavily counterbalanced by the presence of large QCD

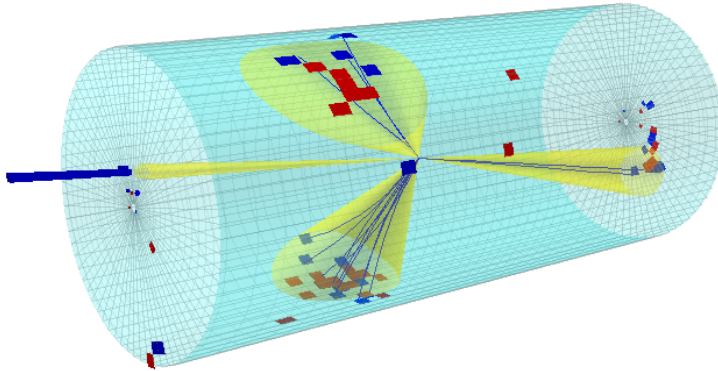


Figure 9. A typical Vector Boson Fusion $H \rightarrow b\bar{b}$ event shown with the DELPHES event display. The event principally contains two forward jets with a large rapidity-gap and two central (b)-jets.

backgrounds at the LHC. Moreover, the presence of pile-up is expected to have a large impact on the jet reconstruction and on the *rapidity gap* requirement. These aspects make this search very challenging, especially at high luminosity, and an ideal playground for testing DELPHES capabilities.

The signal signature is characterized by the presence of two highly energetic jets at high rapidity. Since no color flow is exchanged between the two jets, little hadronic activity is expected in the central part of the detector, besides the Higgs decay products. A typical signal event is shown in figure 9, with the help of the DELPHES event display. In large pile-up scenarios, additional jets might be reconstructed in the central region of the detector, hence spoiling the sensitivity of this search.

Both the signal and background samples have been generated with MADGRAPH5 [9] at a center of mass energy $\sqrt{s} = 14$ TeV. Only the main irreducible $b\bar{b} + jets$ background was considered. Events have been showered and hadronized via PYTHIA6 [16]. Detector simulation and event reconstruction has been performed with DELPHES. Pile-up events originate from a Minimum Bias sample generated with PYTHIA8 [27].

Jets are the only relevant objects to be considered for this analysis. Calorimeter Jets were used. The anti- k_T algorithm with a cone $R = 0.5$ was adopted for clustering calorimeter tower objects. No information on charged pile-up particles is available in Calorimeter Jets, hence the total (charged and neutral) average pile-up contamination density was used for jet pile-up subtraction (see section 4.2). The following event selection was applied:

1. at least 2 b-tagged jets (b_1, b_2) and at least 2 light jets (j_1, j_2) with $p_T > 80, 60, 40, 40$ GeV,
2. $\Delta\eta_{j_1 j_2} > 3, \eta_{j_1} \times \eta_{j_2} < 1, m_{j_1 j_2} > 500$ GeV, no light jets between j_1 and j_2 ,

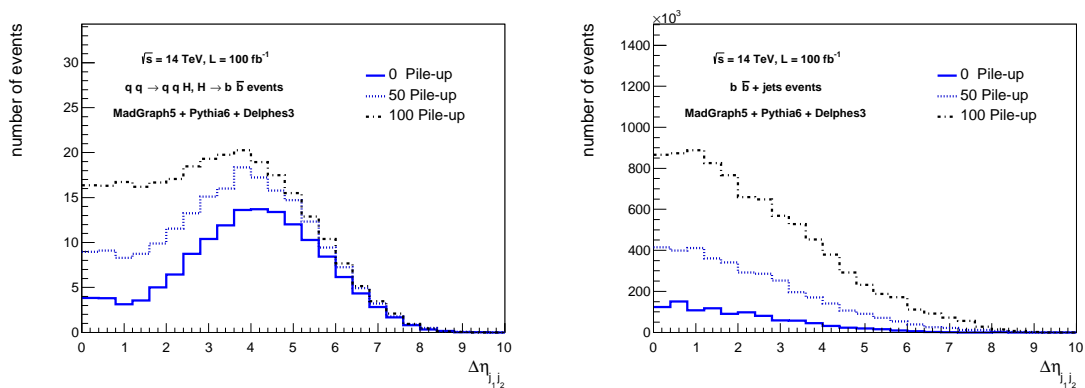


Figure 10. Difference in pseudo-rapidity of the two most energetic reconstructed light jets for the signal (left) and the background (right) with 0, 50 and 100 average pile-up interactions. Histograms are normalized to the expected number of events predicted by MADGRAPH5 at $\sqrt{s} = 14$ TeV for an integrated luminosity of $L = 100 \text{ fb}^{-1}$.

3. $100 < m_{b_1 b_2} < 200 \text{ GeV}$.

The three selection steps are aimed at increasing the signal-to-background ratio. Selection criterion (1) addresses the threshold of the jet momenta. Jets are typically expected to be softer in QCD backgrounds than in the signal, especially the b-jets that, in the signal case, originate from a heavy resonance. Selection (2) addresses specifically the difference in topology between signal and background. The two hardest light jets are required to have a large rapidity gap, a high invariant mass, and no hadronic activity in between, besides the two b's originating from the Higgs decay. Selection (3) further increases the signal purity by requiring a $b\bar{b}$ invariant compatible with the Higgs resonance.

In figure 10 the $\Delta\eta_{j_1 j_2}$ distribution is shown for the signal (left) and background (right) for different pile-up scenarios. The normalization corresponds to the total number of events expected to pass selection (1) for an integrated luminosity $L = 100 \text{ fb}^{-1}$ at $\sqrt{s} = 14$ TeV. As expected, with increasing pile-up, a significant number of additional jets emerges, despite the pile-up subtraction procedure, which leads to an increase in the amount of events passing selection (1). In the signal sample, pile-up jets are then more often wrongly selected as prompt signal jets, leading to a depletion of the rapidity gap. Pile-up also tends to inflate the total background contribution. This aspect is relevant in particular in the tail of the distribution, which corresponds to the signal region.

The total selection efficiency is shown in figure 11 (left) for both signal and background. If jet pile-up subtraction is not applied, the efficiency rapidly grows as a function of pile-up until 20 pile-up interactions and decreases at higher pile-up. The increase is due to the emergence of additional jets, as explained earlier. However, when pile-up and the number of jets become too important, the probability of finding another jet in between the two hardest jets increases, hence drastically decreasing the efficiency of selection (2). It is clear from figure 11 (left) that the pile-up subtraction procedure heavily slows down this effect, allowing for a smoother, but yet still present, dependence on the number of pile-up

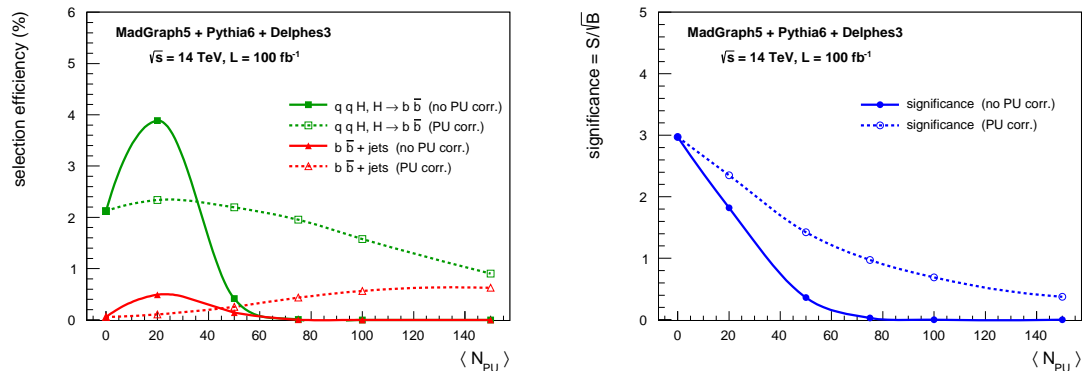


Figure 11. Signal and Background total selection efficiencies (left) and Significance $= \frac{S}{\sqrt{B}}$ (right) as a function of the average number of pile-up interactions, with and without applying jet pile-up subtraction.

interactions. The improvement brought by pile-up subtraction can also be seen on the signal significance in figure 11 (right).

With this example, we have shown that DELPHES can be used to estimate the impact of pile-up on LHC studies. We emphasize that the predictions stated in this short study, should be understood as qualitative rather than quantitative, as indeed, accurate predictions in high pile-up scenarios should solely rely on full simulation tools. On the other hand, it should be noted that no fully parametric study could eventually account for the effects that were illustrated here, unless a prior parametrisation was obtained from a full simulation study. Only simple analysis techniques are used, so that the results are in no way representative of the ultimate potential of the LHC multipurpose detectors.

8 Conclusion

We discussed the version 3.0 of DELPHES, a framework designed to perform a fast and realistic simulation of a general purpose collider experiment. The new modular design of DELPHES was presented, and we described the principles used for modeling the detector and parametrising the event reconstruction.

We showed that DELPHES 3.0 is able to produce realistic observables and is fully validated. It can thus be used to perform quickly realistic physics studies without in-depth knowledge of the technicalities of real experiments.

Acknowledgments

First, we would like to thank Séverine Ovin and Xavier Rouby for their invaluable contribution to the early DELPHES development. We wish to thank the DELPHES users for continuously providing feedback and deep insights. We are very grateful to the MADGRAPH5 team for having integrated DELPHES within MADGRAPH5. Finally, we wish to thank to the members of the CP3 for providing support and useful discussions. We ac-

knowledge the support from the FNRS and the IAP Program, BELSPO VII/37. This work is partly supported by the IISN convention 4.4503.13.

References

- [1] J. Allison, K. Amako, J. Apostolakis, H. Araujo, P. A. Dubois, M. Asai, G. Barrand and R. Capra et al., *Geant4 developments and applications*, IEEE Trans. Nucl. Sci. **53**, 270 (2006).
- [2] S. Ovin, X. Rouby and V. Lemaitre, *DELPHES, a framework for fast simulation of a generic collider experiment*, arXiv:0903.2225 [hep-ph].
- [3] CMS Collaboration, *Particle-Flow Event Reconstruction in CMS and Performance for Jets, Taus, and MET*, CMS-PAS-PFT-09-001.
- [4] M. Cacciari, G. P. Salam and G. Soyez, *FastJet User Manual*, Eur. Phys. J. C **72**, 1896 (2012) [arXiv:1111.6097 [hep-ph]].
- [5] M. Cacciari and G. P. Salam, *Dispelling the N^3 myth for the k_t jet-finder*, Phys. Lett. B **641** (2006) 57 [hep-ph/0512210].
- [6] M. Cacciari, G. P. Salam and G. Soyez, *The Catchment Area of Jets*, JHEP **0804**, 005 (2008) [arXiv:0802.1188 [hep-ph]].
- [7] M. Cacciari and G. P. Salam, *Pileup subtraction using jet areas*, Phys. Lett. B **659**, 119 (2008) [arXiv:0707.1378 [hep-ph]].
- [8] I. Antcheva et al., *A C++ framework for petabyte data storage, statistical analysis and visualization*, Comput. Phys. Commun. **180**, 2499 (2009)
- [9] J. Alwall, M. Herquet, F. Maltoni, O. Mattelaer and T. Stelzer, *MadGraph 5 : Going Beyond*, JHEP **1106**, 128 (2011) [arXiv:1106.0522 [hep-ph]].
- [10] <https://cp3.irmp.ucl.ac.be/projects/ExRootAnalysis>
- [11] S. V. Chekanov, *Next generation input-output data format for HEP using Google's protocol buffers*, arXiv:1306.6675 [cs.CE].
- [12] M. Dobbs, J. Hansen, L. Garren, L. Sonnenschein, *HEPMC User Manual*, <http://lcgapp.cern.ch/project/simu/HepMC>
- [13] L. Garren, P. Lebrun, *StdHep User Manual*, <http://cepa.fnal.gov/psm/stdhep/>
- [14] J. Alwall, A. Ballestrero, P. Bartalini, S. Belov, E. Boos, A. Buckley, J. M. Butterworth and L. Dudko et al., *A Standard format for Les Houches event files*, Comput. Phys. Commun. **176** (2007) 300 [hep-ph/0609017].
- [15] <https://cp3.irmp.ucl.ac.be/projects/delphes>
- [16] T. Sjostrand, S. Mrenna and P. Z. Skands, *PYTHIA 6.4 Physics and Manual*, JHEP **0605**, 026 (2006) [hep-ph/0603175].
- [17] S. Catani, F. Krauss, R. Kuhn and B. R. Webber, *QCD matrix elements + parton showers*, JHEP **0111**, 063 (2001) [hep-ph/0109231].
- [18] CMS Collaboration, *Performance of CMS muon reconstruction in pp collision events at $\sqrt{s} = 7$ TeV*, JINST **7**, P10002 (2012) [arXiv:1206.4071 [physics.ins-det]].
- [19] ATLAS Collaboration, *Expected Performance of the ATLAS Experiment - Detector, Trigger and Physics*, arXiv:0901.0512 [hep-ex].

- [20] CMS Collaboration, *Electron performance with 19.6 fb⁻¹ of data collected at $\sqrt{s} = 8$ TeV with the CMS detector*, CMS-DP-2013-003.
- [21] ATLAS Collaboration, *Jet energy resolution in proton-proton collisions at $\sqrt{s} = 7$ TeV recorded in 2010 with the ATLAS detector*, Eur. Phys. J. C **73**, 2306 (2013) [arXiv:1210.6210 [hep-ex]].
- [22] ATLAS Collaboration, *Performance of Missing Transverse Momentum Reconstruction in ATLAS with 2011 Proton-Proton Collisions at $\sqrt{s} = 7$ TeV*, ATLAS-CONF-2012-101.
- [23] ATLAS Collaboration, *Performance of the ATLAS Inner Detector Track and Vertex Reconstruction in the High Pile-Up LHC Environment*, ATLAS-CONF-2012-042.
- [24] CMS Collaboration, *Measurement of the top-quark mass in $t\bar{t}$ events with lepton+jets final states in pp collisions at $\sqrt{s} = 7$ TeV*, JHEP **1212**, 105 (2012) [arXiv:1209.2319 [hep-ex]].
- [25] <https://cp3.irmp.ucl.ac.be/projects/delphes/wiki/WorkBook/DelphesAnalysis>
- [26] CMS Collaboration, *b-Jet Identification in the CMS Experiment*, CMS-PAS-BTV-11-004.
- [27] T. Sjostrand, S. Mrenna and P. Z. Skands, *A Brief Introduction to PYTHIA 8.1*, Comput. Phys. Commun. **178**, 852 (2008) [arXiv:0710.3820 [hep-ph]].